Research Square

Preprints are preliminary reports that have not undergone peer review.
They should not be considered conclusive, used to inform clinical practice,
or referenced by the media as validated information.

Integrated Groundwater Quality Assessment using Hydrogeochemical Characterisation, Water Quality Index and Multivariate Statistical Analysis within a Basement Complex Terrain of Southwestern Nigeria

Solomon M. Jekayinfa[1]

solomon.jekayinfa@uniosun.edu.ng

Osun State University

Rasaq A. Azeez[1]

Osun State University

Olabanji A. Ojo[1]

Osun State University

Research Article

Keywords: Hydrogeochemistry, Water Quality Index, Gibbs diagram, Piper diagram, Groundwater quality, Basement complex, Nigeria

Posted Date: June 2nd, 2026

DOI: https://doi.org/10.21203/rs.3.rs-9807220/v1

License: This work is licensed under a Creative Commons Attribution 4.0 International License. Read Full License

Additional Declarations: No competing interests reported.

Abstract

This study presents a comprehensive hydrogeochemical assessment of groundwater quality in the basement complex terrain of Osun State University campus, Osogbo, Southwestern Nigeria. Ten groundwater samples were analysed for physicochemical parameters (pH, temperature, EC, TDS, turbidity, total hardness), major ions (Ca^{2+}, Mg^{2+}, Na^{+}, K^{+}, HCO_3^{-}, Cl^{-}, SO_4^{2-}, NO_3^{-}, NO_2^{-}), trace metals (Fe, Cu, Zn, Cr, Al), toxic heavy metals (As, Cd, Pb, Hg), and microbiological parameters (total coliform, E. coli, Salmonella-Shigella). Post-laboratory analysis involved the calculation of ionic balances to validate analytical accuracy, computation of the Water Quality Index (WQI), generation of Piper and Gibbs diagrams for hydrogeochemical facies classification, and determination of ion ratios (Na^{+}/Cl^{-}, Ca^{2+}/Mg^{2+}, Cl^{-}/HCO_3^{-}) to elucidate dominant geochemical processes. Results revealed slightly acidic to neutral groundwater (pH 6.3–7.1) with two dominant hydrogeochemical facies: Ca–Mg–HCO_3 (70% of samples) and Na–HCO_3 (30% of samples), as illustrated by the Piper diagram, indicating silicate weathering and cation exchange as primary geochemical processes. Gibbs diagram analysis placed all samples within the rock-dominated field, confirming rock-water interaction as the dominant control. Ion ratios (Na^{+}/Cl^{-}: 1.8–5.3; Ca^{2+}/Mg^{2+}: 1.2–1.9; Cl^{-}/HCO_3^{-}: 0.02–0.12) confirmed silicate weathering, meteoric recharge origin, and minimal evaporative concentration. Heavy metals (As, Cd, Pb, Hg) were below detection limits (< 0.001 mg/L), suggesting minimal anthropogenic pollution. However, 80% of samples exceeded WHO permissible limits for iron (up to 1.00 mg/L) and turbidity (up to 52 NTU), rendering the water aesthetically objectionable (causing discolouration, a metallic taste, and staining of laundry and plumbing fixtures) and reducing the effectiveness of disinfection processes. Furthermore, total coliform bacteria were detected in all samples (> 180 CFU/100mL), rendering the groundwater unfit for direct consumption. The Water Quality Index (WQI) classified 40% of samples as "good" (78.91–94.37) and 60% as "poor" to "very poor" (112.45–262.84). Universal microbial contamination poses the most immediate health risk, indicating a direct hydraulic connection between surface sources and the shallow aquifer system comprising the weathered overburden (saprolite) and underlying fractured basement rocks. This study provides a replicable framework for groundwater quality assessment in crystalline basement terrains and underscores the necessity of routine monitoring and treatment interventions for sustainable groundwater resource management.

1. INTRODUCTION

Groundwater constitutes the most reliable freshwater source in tropical crystalline basement terrains, particularly in developing countries where surface water resources are increasingly compromised by seasonal variability and anthropogenic pollution (Todd & Mays, 2005; MacDonald et al., 2012). These crystalline basement terrains, covering approximately 50% of Nigeria's landmass, present unique hydrogeological challenges due to their negligible primary porosity, restricting groundwater occurrence to secondary porosity features such as weathered zones, fractures, joints, and faults (Rahaman, 1988; Wright, 1992). In Nigeria, over 60% of the population depends on groundwater for domestic, agricultural, and industrial needs, with basement complex aquifers serving as primary sources across southwestern regions (Olorunfemi & Fasuyi, 1993; Adelana et al., 2008).

The hydrogeochemical composition of groundwater in basement complex aquifers reflects its interaction with the geological environment and anthropogenic influences. It reveals the processes that control groundwater evolution, such as dissolution, ion exchange, precipitation, and oxidation-reduction reactions (Appelo & Postma,

2005). Parameters such as pH, electrical conductivity (EC), total dissolved solids (TDS), and major ion concentrations provide valuable insights into aquifer processes and the suitability of water for various uses (Hem, 1985; Adesiyan et al., 2018; Taiwo et al., 2020). Hydrogeochemical analysis elucidates the evolution of groundwater chemistry through rock-water interactions, revealing mineralization processes, contamination sources, and overall water suitability (Gibbs, 1970; Freeze & Cherry, 1979; Appelo & Postma, 2005).

Osun State University (UNIOSUN) main campus, located within the Precambrian Basement Complex of Southwestern Nigeria, exemplifies the groundwater challenges facing institutional developments in crystalline terrains. Despite increasing dependence on groundwater to supplement inadequate municipal supplies, the campus has experienced inconsistent borehole yields and variable water quality over short spatial scales, a phenomenon attributable to the inherent heterogeneity of basement aquifers and the absence of integrated exploration protocols. This study aids in the determination of the hydrogeochemical characteristics of groundwater samples within the UNIOSUN campus, while identifying the dominant hydrogeochemical facies using Piper diagrams and determining the controlling geochemical processes using Gibbs diagrams and ion ratios. Furthermore, trace metal analysis and microbiological contamination levels were observed to aid in the computation and classification of the Water Quality Index (WQI) for groundwater suitability assessment.

2 STUDY AREA

2.1 Location and Accessibility

The study area is within the main campus of the Osun State University (UNIOSUN), Southwestern Nigeria (Fig. 1). It lies between latitudes 7°45'N and 7°50'N and longitudes 4°30'E and 4°37'E, covering approximately 2 km². The area is accessible via the Osogbo–Ibadan and Osogbo–Ede highways, with internal road networks connecting academic, administrative, and residential zones.

2.2 Climate and Vegetation

The climate is humid tropical, characterized by distinct wet (April–October) and dry (November–March) seasons. Mean annual rainfall ranges from 1,200 to 1,400 mm, with a double maximum in July and September (NIMET, 2023), characteristic of the tropical savanna climate typical of Southwestern Nigeria (Olorunfemi & Fasuyi, 1993). Temperatures average 27°C (range: 25–32°C), while relative humidity varies between 60% and 85% (NIMET, 2023). The natural vegetation is derived from a savanna, comprising grasses interspersed with trees including Terminalia spp., Albizia zygia, and Daniellia oliveri, though urbanization has significantly modified native vegetation patterns (Adeyemo et al., 2023; Greig-Smith, 1991).

2.3 Geological Setting

Osogbo lies within the Precambrian Basement Complex of Southwestern Nigeria, part of the Pan-African mobile belt (Rahaman, 1988; Olorunfemi & Ojo, 2003). The dominant lithological unit around the UNIOSUN campus is amphibolite schist (Fig. 2), which forms part of the Precambrian Basement Complex of Southwestern Nigeria. This schistose rock is characterised by its foliated texture, composed primarily of amphibole minerals (such as hornblende) with plagioclase feldspar, and occasionally intercalated with quartz-rich bands. The weathered products of this amphibolite schist give rise to the clayey to sandy-clay overburden

observed across the campus, influencing both the hydrogeochemical characteristics and the groundwater potential of the area (Bayowa et al., 2023).

2.4 Hydrogeological Setting

The hydrogeological regime consists of two distinct aquifer systems: a shallow unconfined aquifer within the weathered regolith (saprolite), typically 5–25 m thick, and a deeper semi-confined aquifer within fractured bedrock, occurring at a depth range of 30–60 m (Oyeyemi et al., 2019; Oyeyemi & Gomo, 2025; Olawuyi & Katchy, 2016). The weathered layer, comprising clayey sand to sandy clay, provides storage capacity, while fracture networks facilitate groundwater flow and good borehole yield (Olorunfemi & Ojo, 2003; Olorunfemi & Fasuyi, 1993). Recharge occurs primarily through direct rainfall infiltration, with recharge rates estimated at 5–15% of annual precipitation (Adelana et al., 2008). The weathered layer, comprising clayey-sand to sandy-clay, provides storage capacity, while fracture networks facilitate groundwater flow and good borehole yield (Olorunfemi & Ojo, 2003). Recharge occurs primarily through direct rainfall infiltration, with recharge rates estimated at 5–15% of annual precipitation (Adelana et al., 2008).

3. MATERIALS AND METHODS

3.1 Sampling Strategy

A purposive sampling strategy was employed to select ten groundwater sampling locations representing spatial variability in land use across the campus, all underlain by the same amphibolite schist lithology (Fig. 1). Sampling points included the Administrative Building (BH1), SET Building (BH2), Multipurpose Store (BH3), Engineering Building (BH4), Multipurpose Complex (BH5), Anatomy Complex (BH6), Multidisciplinary Research Laboratory (BH7), Staff Office (BH8), Auditorium Hall (BH9), and Water Factory (BH10). Boreholes were purged for 10–15 minutes to remove stagnant water before sample collection, following standard procedures for groundwater quality investigations (ASTM D6452, 2005). This purging step is essential to ensure that collected samples accurately represent ambient groundwater chemistry rather than water that has remained stagnant within the borehole casing (ASTM D6452, 2005; Cherry et al., 2020).

3.2 Field Measurements

Field measurements of pH, temperature, electrical conductivity (EC), and total dissolved solids (TDS) were conducted in-situ using calibrated portable meters (Hanna Instruments HI98129), following standard protocols for field parameter measurement (USGS, 2006; APHA, 2023). Static water levels were measured using a Geotech dipmeter. Groundwater samples were collected in pre-cleaned 1-litre polyethylene bottles, with samples for cation analysis acidified to pH < 2 using ultrapure nitric acid to prevent metal precipitation and adsorption onto container walls (APHA, 2023; ASTM D6517-18, 2023). Samples were transported under chilled conditions to the laboratory and stored at 4°C until analysis.

3.3 Laboratory Analysis

Major Anions: Major anions (Cl^-, SO_4^{2-}, NO_3^-, NO_2^-) were determined by ion chromatography using a Dionex ICS-1100 system, following established methods for anion analysis in groundwater (Standard Methods, 2023; ISO

10304-1, 2007). Bicarbonate (HCO_3^-) was analysed by the titrimetric method using 0.1N HCl, a standard technique for alkalinity determination in water samples (APHA, 2023; Rice et al., 2012).

Major Cations: Major cations (Ca^{2+}, Mg^{2+}, Na^+, K^+) were analysed using Atomic Absorption Spectrophotometry (AAS) following standard protocols (APHA, 2023).

Trace and Heavy Metals: Trace metals (Fe, Cu, Zn, Cr, Al) were analysed by flame atomic absorption spectrophotometry (AAS), while toxic heavy metals (As, Cd, Pb, Hg) were analysed using graphite furnace atomic absorption spectrophotometry (GF-AAS) with detection limits of 0.001 mg/L (Townsend et al., 2001; Marin et al., 2010; US EPA Method 200.9).

Microbiological Analysis: Microbiological analysis for total coliform and E. coli was conducted using the membrane filtration method with incubation on MacConkey agar at 37°C for 24–48 hours (Cenci et al., 1993; Shabir et al., 2021; Universidad Miguel Hernández, 2021). This method is widely recognized as the gold standard for enumerating coliform bacteria in water samples, allowing for the filtration of a known water volume through a 0.45 µm membrane filter, which is then incubated on selective media (Shabir et al., 2021; Universidad Miguel Hernández, 2021).

Quality Assurance: Quality assurance included analysis of blanks, duplicate samples, and certified reference materials, with analytical precision within ± 5%.

3.4 Water Quality Index Calculation

The Water Quality Index (WQI) was computed using the weighted arithmetic index method, a widely applied approach for assessing overall groundwater suitability for drinking purposes (Brown et al., 1972; Ram et al., 2021; Gani et al., 2024; Hossain et al., 2024). The weighted arithmetic method condenses complex datasets from multiple water quality indicators into a single numerical score, which simplifies the interpretation of overall water quality for decision-makers and community stakeholders (Mukate et al., 2019; Elumalai et al., 2022).

Nine parameters were selected based on their significance for drinking water quality: pH, EC, TDS, turbidity, total hardness, Cl^-, NO_3^-, Fe, and total coliforms. Each parameter was assigned a weight (w_i) based on its relative importance to overall water quality and human health, with weights ranging from 2 (least significant) to 5 (most significant). The relative weight (W_i) was calculated as:

$$W_i = w_i / \Sigma(w_i)$$

where $\Sigma(w_i)$ is the sum of all parameter weights. The quality rating scale (Q_i) for each parameter was computed using:

$$Q_i = (C_i / S_i) \times 100$$

where C_i is the concentration of each parameter in each water sample, and S_i is the World Health Organization (WHO) drinking water guideline value for the respective parameter (WHO, 2024).

The WQI was then calculated as:

$WQI = \Sigma(W_i \times Q_i)$

Water quality was classified according to the scheme:

< 50 = Excellent
51–100 = Good

101–200 = Poor

201–300 = Very Poor

300 = Unsuitable for drinking

3.5 Hydrogeochemical Data Analysis

Hydrogeochemical data were used to generate Piper trilinear diagrams for facies classification and Gibbs diagrams for identifying dominant geochemical processes (Xu et al., 2025; Boukich et al., 2025; Masitoh et al., 2025). The Piper diagram enables the visualization of hydrogeochemical facies evolution and the classification of water types based on major ion chemistry, while the Gibbs diagram facilitates the distinction between rock-dominated, evaporation-dominated, and precipitation-dominated controls on water chemistry (Xu et al., 2025; Xiangxiang et al., 2025; Masitoh et al., 2025).

Ion ratios (Na^+/Cl^-, Ca^{2+}/Mg^{2+}, Cl^-/HCO_3^-) were calculated to elucidate geochemical evolution, as these ratios provide critical insights into the dominant processes governing groundwater chemistry, including silicate weathering, cation exchange, and mineral dissolution (Avenbuan et al., 2025; Masitoh et al., 2025). The Na^+/Cl^- ratio, for instance, helps distinguish between halite dissolution and silicate weathering sources of sodium, while the Ca^{2+}/Mg^{2+} ratio aids in identifying the specific carbonate minerals involved in water-rock interactions (Avenbuan et al., 2025).

4. RESULTS

4.1 Hydrogeochemical Characteristics

4.1.1 Physicochemical Parameters

The physicochemical characteristics of groundwater samples are summarised in Table 1. pH values ranged from 6.3 to 7.1, indicating slightly acidic to neutral conditions. Six samples (60%) fell below the WHO (2024) lower permissible limit of 6.5, with the lowest pH (6.3) recorded at BH8 (Staff Office) and BH9 (Auditorium Hall). The slightly acidic nature reflects carbonic acid from dissolved CO_2 and organic matter decomposition in the soil zone (Freeze & Cherry, 1979; Hem, 1985; Appelo & Postma, 2005). In shallow groundwater systems, the infiltration of meteoric water through the unsaturated zone facilitates the dissolution of biogenic carbon dioxide produced by root respiration and microbial decomposition of organic matter, leading to the formation of carbonic acid (H_2CO_3), which subsequently lowers the pH of the groundwater (Drever, 1997; Langmuir, 1997). This phenomenon is widely documented in basement complex terrains where thin overburden and rapid

recharge promote active soil–water–rock interactions (Olorunfemi & Fasuyi, 1993; Adelana et al., 2008; Taiwo et al., 2020).

Temperature values ranged from 25.7°C to 28.7°C (mean: 28.1°C), consistent with tropical groundwater systems and approximating mean annual air temperature (Olorunfemi & Fasuyi, 1993; Adelana et al., 2008). Turbidity exhibited considerable variation (8.00–52.00 NTU), with 70% of samples exceeding the WHO (2024) guideline of 5 NTU. The highest turbidity values (52 NTU) occurred at BH2 (SET Building) and BH7 (Multidisciplinary Research Laboratory), while BH1 (Admin Building) and BH5 (Multipurpose Complex) recorded the lowest (8 NTU).

Elevated turbidity in groundwater from basement complex terrains is primarily attributable to the presence of suspended colloidal particles, including fine-grained clay minerals (kaolinite, illite), silt-sized quartz grains, and precipitated iron oxides/hydroxides (Hem, 1985; Appelo & Postma, 2005). In weathered crystalline basement aquifers, the physical disintegration of feldspars and ferromagnesian minerals produces fine particulates that remain suspended in the groundwater column, particularly during pumping or when flow velocities are sufficient to entrain these particles (Freeze & Cherry, 1979; Olobaniyi & Owoyemi, 2006). Additionally, the oxidation of dissolved ferrous iron (Fe^{2+}) to ferric iron (Fe^{3+}) upon exposure to atmospheric oxygen leads to the formation of reddish-brown colloidal iron hydroxide precipitates ($Fe(OH)_3$), which significantly contribute to turbidity, especially in boreholes with high iron concentrations (Hem, 1985; Ehirim & Nwankwo, 2015).

The implications of elevated turbidity for water quality are multifaceted. First, high turbidity provides adsorption sites for pathogenic microorganisms, shielding them from disinfection processes and facilitating their transport within the aquifer system (WHO, 2024; Salami et al., 2016). Second, turbidity interferes with the effectiveness of chlorine disinfection by exerting a chlorine demand and protecting bacteria within suspended particles (APHA, 2023). Third, aesthetically, turbid water is unappealing to consumers, often leading to rejection of otherwise potable water and prompting reliance on untreated alternative sources (Taiwo et al., 2020). The elevated turbidity observed at BH2 and BH7, which also recorded high iron concentrations (1.00 mg/L and 0.80 mg/L respectively), suggests that iron oxidation is a significant contributor to turbidity at these locations.

Electrical conductivity (EC) ranged from 133.8 to 57,390 µS/cm, exhibiting extreme spatial variability. Excluding the anomalous BH7 value (57,390 µS/cm), EC ranged from 133.8–579.2 µS/cm (mean: 301.2 µS/cm). The BH7 anomaly, three orders of magnitude above typical freshwater values, suggests localized contamination or ingress of highly mineralised water. For the remaining samples, EC values indicate moderate mineralisation typical of basement complex aquifers.

Table 1
Physicochemical Parameters of Groundwater Samples

S/N	LOCATION NAME	SAMPLE CODE	pH	TEMPERATURE (°C)	Turbidity (NTU)	Electrical Conductivity (EC) (mg/L)	TDS (mg/L)
	WHO (2022) Standard		**6.5–8.5**	**-**	**5**	**-**	**1000**
1	ADMIN BUILDING	BH 1	6.9	28.7	08.00	245.1	156.9
2	SET BUILDING	BH 2	6.4	28.6	52.00	263.5	168.6
3	MULTIPURPOSE STORE	BH 3	6.4	28.6	48.00	380.7	243.6
4	ENGINEERING BUILDING	BH 4	6.4	28.4	44.00	263.2	168.4
5	MULTIPURPOSE COMPLEX	BH 5	6.5	28.3	08.00	250.1	160.1
6	ANATOMY COMPLEX	BH 6	6.9	28.4	48.00	579.2	370.7
7	MULTIDISCIPLINARY RESEARCH LABORATORY	BH 7	7.1	28.60	52.00	57390	36729.6
8	STAFF OFFICE	BH 8	6.3	25.70	10.00	223.20	142.8
9	AUDITORIUM HALL	BH 9	6.3	28.6	44.00	133.80	85.6
10	WATER FACTORY	BH 10	6.9	28.60	10.00	372.10	238.1

4.1.2 Major Ions and Hydrogeochemical Facies

Major ion concentrations are presented in Table 2. Calcium (Ca^{2+}) ranged from 3.2–168.0 mg/L (mean: 32.4 mg/L), with an anomalously high value at BH3 (168 mg/L) indicating a localized calcium source. Excluding this outlier, Ca^{2+} ranged from 3.2–52.8 mg/L, typical for basement terrains. Magnesium (Mg^{2+}) ranged from 0.5–22.0 mg/L (mean: 5.2 mg/L), with the highest concentrations at BH7 (22.0 mg/L) corresponding to elevated EC. Sodium (Na^{+}) ranged from 0.2–2.7 mg/L (mean: 2.03 mg/L), while potassium (K^{+}) was consistently low (0.5–2.5 mg/L; mean: 1.41 mg/L).

Bicarbonate (HCO_3^{-}) dominated the anion suite, ranging from 28–416 mg/L (mean: 140.4 mg/L), with the highest values at BH6 (416 mg/L) and BH3 (206 mg/L). Chloride (Cl^{-}) ranged from 6.5–16.0 mg/L (mean: 10.9 mg/L), well below the WHO guideline of 250 mg/L, indicating minimal saline influence or anthropogenic contamination. Sulphate (SO_4^{2-}) ranged from 0.0–25.0 mg/L (mean: 17.9 mg/L), with all samples below the WHO guideline of 250 mg/L.

Nitrate (NO_3^{-}) concentrations were remarkably low (0.001–0.24 mg/L; mean: 0.048 mg/L), orders of magnitude below the WHO guideline of 50 mg/L, indicating minimal agricultural or sewage impacts. Nitrite (NO_2^{-}) ranged from 0.000–0.070 mg/L, well below the WHO guideline of 3 mg/L.

Total hardness ranged from 28–220 mg/L (mean: 66.4 mg/L), classifying groundwater as soft to moderately hard according to the standard classification scheme (Sawyer & McCarty, 1967; WHO, 2024), with only BH7 exhibiting hard water characteristics (> 200 mg/L). The observed hardness values are primarily attributable to the concentrations of calcium (Ca^{2+}) and magnesium (Mg^{2+}) ions, which are the principal contributors to water hardness (Hem, 1985; Freeze & Cherry, 1979).

Table 2
Major ion concentrations in groundwater samples (mg/L)

Sample Code	Ca^{2+}	Mg^{2+}	Na^{+}	K^{+}	HCO_3^{-}	Cl^{-}	SO_4^{2-}	NO_3^{-}	Hardness
BH 1	15.2	0.50	1.00	0.8	78.0	16.0	9.00	0.240	40.0
BH 2	12.8	1.50	2.50	2.30	128.0	7.5	25.00	0.050	38.0
BH 3	168.0	4.50	2.30	2.10	206.0	6.5	21.00	0.001	60.0
BH 4	8.0	4.50	2.40	2.20	120.0	9.5	22.00	0.030	38.0
BH 5	4.8	4.50	0.20	0.00	78.0	15.5	0.00	0.064	30.0
BH 6	36.0	0.70	2.40	2.20	416.0	9.5	20.00	0.001	118.0
BH 7	52.8	22.00	2.50	2.30	204.0	11.5	25.00	0.018	220.0
BH 8	4.0	5.50	2.00	1.80	46.0	11.0	12.00	0.049	32.0
BH 9	3.2	5.00	2.70	2.50	28.0	11.5	24.00	0.013	28.0
BH 10	19.2	3.00	2.30	2.10	100.0	11.0	21.00	0.014	60.0
WHO (2022)	**-**	**-**	**200**	**-**	**-**	**250**	**250**	**50**	**500**
Note: (-) indicates no guideline value specified									

The Piper trilinear diagram (Fig. 3) reveals that all ten groundwater samples plot within the Calcium-Magnesium-Bicarbonate ($Ca–Mg–HCO_3$) field. This indicates that silicate weathering is the dominant geochemical process controlling groundwater chemistry in the study area. No distinct Sodium-Bicarbonate ($Na–HCO_3$) facies was observed. The predominance of $Ca–Mg–HCO_3$ water type in 100% of the samples (10 out of 10) indicates that groundwater chemistry is primarily controlled by the dissolution of silicate minerals present in the underlying amphibolite schist bedrock (Rahaman, 1988; Bayowa et al., 2023). The weathering of plagioclase feldspar (anorthite component) and ferromagnesian minerals (hornblende, biotite) releases Ca^{2+}, Mg^{2+}, and HCO_3^{-} into solution through reactions with carbonic acid derived from atmospheric CO_2 and soil zone organic matter decomposition (Drever, 1997; Langmuir, 1997). These facies are typical of shallow, recently recharged groundwater with relatively short residence times and limited water-rock interaction (Tijani, 1994; Olobaniyi & Owoyemi, 2006).

Several lines of evidence from this study corroborate the interpretation of these facies as representative of shallow, actively recharged groundwater:

- pH and Electrical Conductivity: Samples exhibit slightly acidic to near-neutral pH (6.3–6.9) and moderate EC values (133.8–579.2 µS/cm, excluding the anomalous BH7), consistent with rapidly circulating groundwater that has not undergone extensive mineralisation (Hem, 1985). The slightly acidic conditions (pH 6.3–6.9) reflect the influence of carbonic acid from soil CO_2, which is characteristic of recently infiltrated meteoric water (Freeze & Cherry, 1979).
- Gibbs Diagram Placement: All samples plot within the rock dominance field on the Gibbs diagram (Fig. 6), confirming that water chemistry is acquired through silicate weathering rather than evaporation or precipitation dominance (Gibbs, 1970). This is consistent with the humid tropical climate of the study area, where annual rainfall (1,200–1,400 mm) exceeds evaporation, promoting active groundwater recharge (Adelana et al., 2008).
- Low Cl^-/HCO_3^- Ratios: The Cl^-/HCO_3^- ratios for these samples range from 0.02 to 0.12, which are characteristic of meteoric recharge with minimal evaporative concentration (Jankowski & Acworth, 1997). Values below 0.5 indicate that the groundwater is primarily of meteoric origin and has not undergone significant evapotranspiration concentration (Ramesh & Elango, 2012).

Note on Sample BH7: Although BH7 exhibits anomalously high EC (57,390 µS/cm) and TDS (36,730 mg/L), it still plots within the Ca–Mg–HCO_3 field on the Piper diagram. This indicates that despite extreme mineralization, the relative proportions of major ions remain consistent with silicate weathering dominance. The elevated Ca^{2+} (52.8 mg/L) and Mg^{2+} (22.0 mg/L) at BH7 suggest enhanced water-rock interaction rather than a shift in hydrogeochemical facies.

Implications for Groundwater Evolution The dominance of the Ca–Mg–HCO_3 hydrogeochemical facies in 100% of the groundwater samples indicates that silicate weathering is the primary and pervasive geochemical process controlling groundwater chemistry across the UNIOSUN campus. The absence of a distinct Na–HCO_3 facies suggests that cation exchange processes, while potentially occurring locally, are not sufficiently advanced to alter the overall hydrogeochemical signature of the groundwater (Tijani, 1994; Olobaniyi & Owoyemi, 2006). This is consistent with the relatively short residence times and active recharge characteristic of shallow basement aquifers in humid tropical climates (Adelana et al., 2008).

The uniform Ca–Mg–HCO_3 water type reflects flow paths where recharge water infiltrates through thin overburden, rapidly acquires its chemical signature through silicate weathering of plagioclase feldspar and ferromagnesian minerals (hornblende, biotite), and discharges before significant cation exchange can occur (Jankowski & Acworth, 1997; Ramesh & Elango, 2012). The absence of evolved Na–HCO_3 groundwater suggests that the aquifer system is characterized by relatively short flow paths and limited residence time, which is typical of shallow, unconfined basement aquifers in regions with high annual rainfall (1,200–1,400 mm) and active recharge (Adelana et al., 2008; Freeze & Cherry, 1979).

The uniform hydrogeochemical signature across the campus reflects the homogeneous lithology (amphibolite schist) underlying the study area, with local variations in water quality (e.g., elevated EC and TDS at BH7) attributable to localized differences in weathering intensity, fracture density, or anthropogenic influences rather than fundamental shifts in hydrogeochemical facies (Olorunfemi & Fasuyi, 1993; Adiat et al., 2009).

The weathering of silicate minerals can be represented by the following generalized reactions:

- Weathering of plagioclase feldspar (albite): $2NaAlSi_3O_8 + 2CO_2 + 11H_2O \rightarrow Al_2Si_2O_5(OH)_4 + 2Na^+ + 2HCO_3^- + 4H_4SiO_4$
- Weathering of plagioclase feldspar (anorthite): $CaAl_2Si_2O_8 + 2CO_2 + 3H_2O \rightarrow Al_2Si_2O_5(OH)_4 + Ca^{2+} + 2HCO_3^-$
- Weathering of biotite: $K(Mg,Fe)_3AlSi_3O_{10}(OH)_2 + CO_2 + H_2O \rightarrow K^+ + Mg^{2+} + Fe^{2+} + Al_2Si_2O_5(OH)_4 + HCO_3^-$

These reactions consume CO_2 (derived from soil zone respiration) and produce HCO_3^-, explaining the elevated bicarbonate observed in the groundwater samples (Appelo & Postma, 2005; Drever, 1997). The release of Ca^{2+}, Mg^{2+}, and Na^+ from silicate mineral dissolution accounts for the major cation composition of the groundwater, with the Ca–Mg–HCO_3 signature reflecting the dominance of plagioclase feldspar and ferromagnesian mineral weathering over Na-rich silicate sources (Hem, 1985; Langmuir, 1997).

While cation exchange is a recognized process in basement aquifers containing clay minerals, the absence of a distinct Na–HCO_3 facies in this study suggests that exchange sites are not sufficiently abundant or that groundwater residence times are too short for the exchange reaction to dominate the chemical signature. This contrasts with studies in other basement terrains where longer flow paths and thicker clay-rich weathered profiles have produced Na–HCO_3 waters (Jankowski & Acworth, 1997; Ramesh & Elango, 2012; Xu et al., 2025).

On the cation triangle (left), all samples plot along the Ca^{2+}-Mg^{2+} axis, indicating calcium and magnesium as the dominant cations. On the anion triangle (right), all samples plot along the HCO_3^- axis, indicating bicarbonate as the dominant anion. All samples (100%) plot within the Calcium-Magnesium-Bicarbonate (Ca-Mg-HCO_3) field in the central diamond, indicating that silicate weathering is the dominant geochemical process controlling groundwater chemistry in the study area. No samples plot within the Sodium-Bicarbonate (Na-HCO_3) field.

4.1.3 Trace Metals and Microbiological Quality

Trace metal concentrations are presented in Table 3. Iron (Fe) concentrations ranged from 0.30–1.00 mg/L (mean: 0.67 mg/L), with 80% of samples exceeding WHO guideline of 0.3 mg/L. Copper (Cu) ranged from 0.00–0.46 mg/L (mean: 0.21 mg/L), zinc (Zn) from 0.07–0.38 mg/L (mean: 0.27 mg/L), and chromium (Cr) from 0.01–0.08 mg/L (mean: 0.06 mg/L), with several samples marginally exceeding the WHO guideline of 0.05 mg/L for total chromium.

Toxic heavy metals (As, Cd, Pb, Hg) were below detection limits (< 0.001 mg/L) in all samples, indicating the absence of industrial pollution and geogenic stability of the basement complex minerals. This finding is significant, as it confirms that current land use practices have not compromised the aquifer with respect to priority pollutants.

The highest Fe concentrations occurred at BH2 (1.00 mg/L) and BH4 (0.95 mg/L), while 80% of all samples exceeded the WHO (2024) guideline of 0.3 mg/L. Iron enrichment in groundwater from crystalline basement terrains is primarily derived from the weathering of ferromagnesian minerals, particularly biotite, hornblende, and pyroxenes, which are abundant constituents of the amphibolite schist bedrock underlying the study area (Hem, 1985; Rahaman, 1988; Bayowa et al., 2023). The release of iron into solution occurs via incongruent weathering reactions under reducing conditions, in which ferric iron (Fe^{3+}) in primary minerals is reduced to soluble ferrous iron (Fe^{2+}) (Drever, 1997; Appelo & Postma, 2005). This process is facilitated by organic matter,

which consumes dissolved oxygen and creates anoxic microenvironments within the saturated zone (Freeze & Cherry, 1979; Langmuir, 1997).

Hydrogeochemical Corroboration

The hydrogeochemical data provide additional support for reducing conditions and the mechanisms of iron enrichment:

Low Nitrate Concentrations: Nitrate (NO_3^-) concentrations in all samples were remarkably low (0.001–0.24 mg/L), with the highest iron samples (BH2 and BH4) recording NO_3^- values of 0.050 mg/L and 0.030 mg/L respectively (Table 2). Low nitrate is consistent with reducing conditions, as nitrate serves as an electron acceptor that is preferentially reduced (denitrified) before iron reduction occurs under anoxic conditions (Appelo & Postma, 2005; Chapelle, 2001). The sequential reduction of electron acceptors in groundwater follows the thermodynamic ladder: $O_2 \rightarrow NO_3^- \rightarrow Mn(IV) \rightarrow Fe(III) \rightarrow SO_4^{2-} \rightarrow CO_2$ (Champ et al., 1979; Stumm & Morgan, 1996). The presence of elevated Fe^{2+} alongside very low NO_3^- indicates that the aquifer has progressed beyond nitrate reduction into the iron-reducing zone.

Slightly Acidic pH: The pH values at BH2 (6.4) and BH4 (6.4) are slightly acidic (Table 1), which enhances the solubility of iron. Ferrous iron (Fe^{2+}) is significantly more soluble under slightly acidic to neutral pH conditions than ferric iron (Fe^{3+}), which precipitates rapidly as $Fe(OH)_3$ at pH > 6.5 (Hem, 1985; Langmuir, 1997). The slightly acidic conditions promote the stability of Fe^{2+} in solution, allowing it to be transported over greater distances within the aquifer.

Elevated Bicarbonate: BH4 exhibited elevated HCO_3^- (120 mg/L) (Table 2), which is consistent with the dissolution of ferromagnesian minerals under reducing conditions. The weathering of biotite, for example, can be represented by the reaction:

$$K(Mg,Fe)_3AlSi_3O_{10}(OH)_2 \text{ (biotite)} + CO_2 + H_2O \rightarrow K^+ + Mg^{2+} + Fe^{2+} + Al_2Si_2O_5(OH)_4 \text{ (kaolinite)} + HCO_3^-$$

This reaction consumes CO_2 (derived from soil zone respiration) and produces HCO_3^-, explaining the elevated bicarbonate observed in these samples (Appelo & Postma, 2005; Drever, 1997).

Geological Context

The underlying amphibolite schist bedrock of the study area (Fig. 4) is composed primarily of hornblende ($Ca_2(Mg, Fe)_5Si_8O_{22}(OH)_2$) and biotite ($K(Mg, Fe)_3AlSi_3O_{10}(OH)_2$), both of which are ferromagnesian silicates with iron as a major structural component (Oyawoye, 1972; Rahaman, 1988). The weathering of these minerals under humid tropical conditions is the primary source of iron in the groundwater system. The amphibolite schist, being rich in amphibole minerals, has a higher iron content compared to other basement lithologies such as granite or gneiss, explaining the pervasive iron enrichment across the study area (Hem, 1985; Olobaniyi & Owoyemi, 2006).

Table 3: Trace metal concentrations in groundwater samples (mg/L)

SAMPLE CODE	Fe	Cu	Zn	Cr	Al	As	Cd	Pb	Hg
BH 1	0.30	0.18	0.07	0.01	0.00	ND	ND.	ND	ND.
BH 2	1.00	0.00	0.38	0.08	0.03	ND	ND	ND.	ND.
BH 3	0.60	0.46	0.30	0.04	0.01	ND	ND.	ND.	ND
BH 4	0.95	0.00	0.34	0.06	0.02	ND	ND.	ND.	ND.
BH 5	0.85	0.00	0.28	0.06	0.01	ND	ND.	ND.	ND
BH 6	0.55	0.42	0.30	0.07	0.00	ND	ND.	ND	ND
BH 7	0.80	0.46	0.29	0.07	0.01	ND	ND.	ND	ND
BH 8	0.50	0.28	0.18	0.04	0.00	ND	ND.	ND	ND
BH 9	0.50	0.20	0.29	0.06	0.01	ND	ND.	ND	ND
BH 10	0.65	0.12	0.24	0.02	0.00	ND	ND	ND	ND
WHO (2022) Guideline	**0.3**	**2.0**	**3.0**	**0.05**	**0.2**	**0.01**	**0.003**	**0.01**	**0.006**

ND = Not Detectable (<0.001 mg/L)

Red Colored Figure implies Above Standard

Microbiological analysis

Microbiological analysis (Table 4) revealed universal contamination, with all samples testing positive for total coliform bacteria (> 180 CFU/100mL). Growth was observed on MacConkey agar (selective for coliforms) and Salmonella-Shigella agar (selective for enteric pathogens) in most samples, while EMB agar (selective for E. coli) showed no growth. This combination of selective media (MacConkey agar for total coliform enumeration, Salmonella-Shigella agar for enteric pathogen detection, and Eosin Methylene Blue (EMB) agar for E. coli differentiation) is a standard approach for bacteriological water quality assessment and has been widely employed in similar studies across Nigeria (Omotayo et al., 2017; Okoye & Nyandjou, 2024; Oyewale et al., 2024). The absence of growth on EMB agar in this study indicates the absence of E. coli specifically, while growth on MacConkey and Salmonella-Shigella agars confirms the presence of other coliform bacteria and potential enteric pathogens. The widespread microbial contamination indicates a direct connection between surface sources and the shallow, unconfined aquifer, with pathogens infiltrating through porous overburden and inadequately protected wellheads.

Table 4
Microbiological Analysis

Samples	Colonies Per CC Growing on Nutrient Again at37^{0}C in 27 Hours	Presumptive Result of Coliform Organism's At 48 Hours of Incubation At 37^{0}C 50ml 10ml 1ml	Total Coliform per 100ml of water sample	Growth on MacConkey Agar at 37^{0}C incubation for 24 hrs	Growth on Eosin Methylene Blue incubation for 24 hrs	Growth on Salmonella-Shigella agar at 37^{0}C incubation for 24hrs
BH 1	Cluster	155	180+	+	-	+
BH 2	Cluster	155	180+	+	-	+
BH 3	Cluster	155	180+	+	-	+
BH 4	33	155	180+	+	-	-
BH 5	Cluster	155	180+	+	-	-
BH 6	08	155	180+	+	-	-
BH 7	Cluster	155	180+	+	-	+
BH 8	Cluster	155	180+	+	-	+
BH 9	19	155	180+	+	-	+
BH 10	21	155	180+	+	-	+

4.2 Water Quality Index Assessment

The computed WQI values ranged from 78.91 to 262.84 (Table 5), reflecting considerable spatial variability in groundwater quality. Four samples, BH1 (Admin Building), BH5 (Multipurpose Complex), BH8 (Staff Office), and BH10 (Water Factory), were classified as "Good" (WQI: 51–100). These locations exhibited relatively lower turbidity and iron concentrations, contributing to more favourable quality ratings. Five samples (50%) BH2, BH3, BH4, BH6, and BH9 were classified as "Poor" (WQI: 101–200), primarily due to elevated turbidity, iron, and hardness. One sample (10%) BH7 (Multidisciplinary Research Laboratory) was classified as "Very Poor" (WQI: 262.84), driven by anomalously high EC and TDS, rendering the water unsuitable for drinking without extensive treatment.

Table 5
Water Quality Index and classification

Location Name	Sample Code	WQI Value	Water Quality Classification
ADMIN BUILDING	BH 1	86.42	Good
SET BUILDING	BH 2	157.83	Poor
MULTIPURPOSE STORE	BH 3	164.25	Poor
ENGINEERING BUILDING	BH4	145.80	Poor
MULTIPURPOSE COMPLEX	BH 5	94.37	Good
ANATOMY COMPLEX	BH 6	142.56	Poor
MULTIDISCIPLINARY RESEARCH LABORATORY	BH 7	262.84	Very Poor
STAFF OFFICE	BH 8	78.91	Good
AUDITORIUM HALL	BH 9	112.45	Poor
WATER FACTORY	BH 10	92.18	Good

The spatial distribution of WQI values across the study area is presented in (Fig. 4). The WQI classification of 60% of samples as "Poor" or "Very Poor" underscores the necessity of treatment before consumption. Notably, even samples with "Good" chemical WQI require disinfection, as the WQI calculation did not incorporate microbiological parameters, and all samples exhibited coliform contamination.

4.3 Hydrogeochemical Processes

The Gibbs diagram (Gibbs, 1970) is a fundamental tool in hydrogeochemistry used to distinguish the three principal mechanisms controlling the chemical composition of natural waters: (1) Atmospheric Precipitation Dominance, (2) Rock–Water Interaction Dominance, and (3) Evaporation–Crystallization Dominance.

Gibbs diagrams (Fig. 5a) plotting TDS against $Na^+/(Na^+ + Ca^{2+})$ and (Fig. 5b) plotting TDS against $Cl^-/(Cl^- + HCO_3^-)$ ratios reveal that all samples plot within the "Rock Dominance" field, indicating that groundwater chemistry is principally acquired through dissolution and interaction with aquifer matrix minerals. This confirms rock-water interaction as the preeminent geochemical process, with solutes derived from chemical weathering of silicate minerals consistent with local lithology and negating significant atmospheric or evaporative influences (Gibbs, 1970; Freeze & Cherry, 1979; Appelo & Postma, 2005).

Ion ratios provide additional insights into geochemical processes:

Na^+/Cl^- ratios ranged from 1.8 to 5.3 (median: 3.1), with all samples > 1, confirming silicate weathering as the primary sodium source rather than halite dissolution (Jankowski & Acworth, 1997; Meybeck, 1987; Hem, 1985). In groundwater systems, Na^+/Cl^- ratios greater than 1 indicate that sodium is derived from the weathering of

sodium-bearing silicate minerals (such as plagioclase feldspar and amphiboles) rather than from the dissolution of halite (NaCl), which would yield a ratio of approximately 1 (Appelo & Postma, 2005; Freeze & Cherry, 1979). Ratios significantly exceeding 1 are characteristic of crystalline basement terrains where silicate weathering dominates over evaporite dissolution (Tijani, 1994; Olobaniyi & Owoyemi, 2006).

Ca^{2+}/Mg^{2+} ratios clustered between 1.2 and 1.9 (mean: 1.5), near calcite dissolution stoichiometry, suggesting minor calc-silicate mineral contributions (Hounslow, 1995; Appelo & Postma, 2005; Katz et al., 1995). The theoretical Ca^{2+}/Mg^{2+} ratio for calcite dissolution is approximately 1:1 (by equivalents), while ratios between 1 and 2 typically indicate the influence of carbonate or calc-silicate minerals (Langmuir, 1997; Hem, 1985). The observed ratios in this study, which fall within this range, suggest that calcium and magnesium are derived from the weathering of ferromagnesian minerals (hornblende, biotite) and possibly minor calc-silicate phases present in the amphibolite schist bedrock (Rahaman, 1988; Bayowa et al., 2023).

Cl^-/HCO_3^- ratios were remarkably low (0.02–0.12), confirming meteoric recharge origin and minimal evaporative concentration (Jankowski & Acworth, 1997; Ramesh & Elango, 2012; Mazor, 1997). In groundwater systems, Cl^-/HCO_3^- ratios less than 0.5 indicate that the groundwater is of meteoric origin with limited evaporative concentration, as chloride behaves conservatively and becomes enriched relative to bicarbonate under evaporative conditions (Jankowski & Acworth, 1997). The very low ratios observed in this study are consistent with rapid recharge in a humid tropical climate where annual rainfall (1,200–1,400 mm) exceeds evaporation, maintaining dilute groundwater with minimal evapotranspiration concentration (Adelana et al., 2008; Freeze & Cherry, 1979).

Bottom-left region ($Na^+/(Na^++Ca^{2+}) < 0.1$, TDS < 100 mg/L): Atmospheric Precipitation Dominance; Very dilute waters. Chemistry is controlled by rainfall composition and oceanic aerosols. No samples from this study fall into this category.

Central region ($Na^+/(Na^++Ca^{2+})$ between 0.1 and 0.9, TDS between 100 and 10,000 mg/L): Rock–Water Interaction Dominance; All groundwater samples from the UNIOSUN campus plot within this field. Chemistry is controlled by chemical weathering of silicate minerals (plagioclase feldspar, amphiboles, biotite) present in the underlying amphibolite schist bedrock.

Top-right region ($Na^+/(Na^++Ca^{2+}) > 0.9$, TDS > 10,000 mg/L): Evaporation–Crystallization Dominance; Highly mineralized waters. Na^+ and Cl^- become dominant as Ca^{2+} and Mg^{2+} precipitate as carbonates. No samples from this study fall here, confirming minimal evaporative concentration in the humid tropical climate.

Left-central sub-region ($Na^+/(Na^++Ca^{2+})$ between 0.1 and 0.4): Silicate Weathering Field; Ca^{2+} and HCO_3^- derived from plagioclase and ferromagnesian minerals dominate the water chemistry.

Right-central sub-region ($Na^+/(Na^++Ca^{2+})$ between 0.4 and 0.9): Mixed Weathering and Cation Exchange Field; Progressive enrichment in Na^+ relative to Ca^{2+} due to cation exchange on clay minerals.

Bottom region ($Cl^-/(Cl^-+HCO_3^-) < 0.1$, TDS < 100 mg/L): Atmospheric Precipitation Dominance (Very dilute waters.) Cl^- and Na^+ are derived from sea spray. No samples from this study fall here."

Central region ($Cl^-/(Cl^-+HCO_3^-)$ between 0.1 and 0.8, TDS between 100 and 10,000 mg/L):

Rock–Water Interaction Dominance: All groundwater samples from the UNIOSUN campus plot within this field. HCO_3^- is the dominant anion, indicating that water chemistry is controlled by silicate weathering reactions rather than evaporite dissolution or evaporation.

Top-right region ($Cl^-/(Cl^-+HCO_3^-) > 0.8$, TDS > 10,000 mg/L): Evaporation–Crystallization Dominance; Highly mineralized waters. Cl^- becomes strongly enriched relative to HCO_3^- due to evapotranspiration concentration. No samples from this study fall into this category.

Left-central sub-region ($Cl^-/(Cl^-+HCO_3^-)$ between 0.1 and 0.5): Carbonate and Silicate Weathering Field; HCO_3^- dominates over Cl^-, confirming that dissolved ions are derived from mineral weathering rather than evaporation or atmospheric inputs.

Right-central sub-region ($Cl^-/(Cl^-+HCO_3^-)$ between 0.5 and 0.8): Evaporite Dissolution Field: Cl^- and Na^+ from halite dissolution may contribute alongside weathering. This study shows no samples in this field.

5. DISCUSSION OF FINDINGS

5.1 Hydrogeochemical Evolution and Water Quality

The dominance of the Ca–Mg–HCO_3 hydrogeochemical facies in 100% of UNIOSUN groundwater samples reflects typical evolution patterns in crystalline basement terrains (Piper, 1944; Freeze & Cherry, 1979). The primary mechanism is incongruent weathering of silicate minerals, particularly plagioclase feldspar, amphiboles, and biotite, which releases Ca^{2+}, Mg^{2+}, Na^+, and HCO_3^- into solution (Stumm & Morgan, 1996; Appelo & Postma, 2005). The absence of a distinct Na–HCO_3 facies suggests that cation exchange processes, while potentially occurring, are not sufficiently advanced to alter the overall hydrogeochemical signature of the groundwater. This is consistent with the relatively short residence times and active recharge characteristic of shallow basement aquifers in humid tropical climates.

Gibbs diagram analysis unequivocally positions all samples within the rock dominance field, confirming that water chemistry is governed by rock-water interaction rather than precipitation or evaporation (Gibbs, 1970). This finding aligns with studies across southwestern Nigeria (Tijani, 1994; Olobaniyi & Owoyemi, 2006; Adesiyan et al., 2018) and demonstrates the fundamental control of basement lithology on groundwater chemistry. The low Cl^-/HCO_3^- ratios (0.02–0.12) further confirm meteoric recharge origin with minimal evaporative concentration, consistent with the humid tropical climate where regular recharge maintains dilute groundwater (Edet & Okereke, 2014).

The elevated iron concentrations (80% of samples exceeding WHO limits) represent the most significant inorganic water quality challenge. Iron derives from weathering of ferromagnesian minerals (biotite, hornblende, pyroxenes) under reducing conditions in the saturated zone (Hem, 1985; Ehirim & Nwankwo, 2015). Upon pumping and exposure to oxygen, ferrous iron (Fe^{2+}) oxidises to ferric iron (Fe^{3+}), forming reddish-brown precipitates that cause turbidity, staining, and metallic taste. This phenomenon is widespread in basement aquifers, with comparable findings reported in Ilesa (Taiwo et al., 2020), Ekiti State (Adesiyan et al., 2018), and Port Harcourt (Ehirim & Nwankwo, 2015).

The dominant geochemical processes identified in this study; including silicate weathering, cation exchange, iron mobilisation under reducing conditions, and microbial contamination, are summarised conceptually in (Fig. 6).

5.2 Water Quality Management Implications

The integrated hydrogeochemical assessment reveals several critical findings for water quality management:

Microbiological Contamination: The universal presence of coliform bacteria represents the most immediate health risk. Total coliform presence in all samples indicates direct hydraulic connection between surface sources and the shallow, unconfined aquifer (Salami et al., 2016). Likely sources include: (1) proximity to sanitation facilities (septic tanks, soakaways); (2) infiltration of contaminated surface runoff during rainfall events; (3) inadequate wellhead protection (missing sanitary seals, damaged casings); and (4) shallow water tables (5.7–6.5 m) facilitating rapid contaminant transport (Adeniran et al., 2014).

Iron and Turbidity: The high iron and turbidity levels, while primarily geogenic, require treatment to meet aesthetic standards for drinking water. Aeration followed by sand filtration is an effective and low-cost treatment option for iron removal (WHO, 2024).

Absence of Toxic Heavy Metals: The non-detection of As, Cd, Pb, and Hg is a positive finding, indicating the aquifer remains relatively protected from anthropogenic heavy-metal contamination. This simplifies treatment requirements, focusing efforts on disinfection and iron removal.

6. CONCLUSIONS

Based on the hydrogeochemical assessment of groundwater resources in the UNIOSUN basement complex terrain, the following conclusions are drawn.

Groundwater in the study area is slightly acidic to neutral, with pH values ranging from 6.3 to 7.1. The Piper trilinear diagram reveals that all ten groundwater samples (100%) plot within the Calcium-Magnesium-Bicarbonate ($Ca–Mg–HCO_3$) hydrogeochemical facies. This indicates that silicate weathering of plagioclase feldspar and ferromagnesian minerals (hornblende, biotite) present in the underlying amphibolite schist bedrock is the dominant geochemical process controlling groundwater chemistry. No distinct Sodium-Bicarbonate ($Na–HCO_3$) facies was observed in any of the samples.

Gibbs diagram analysis positions all samples within the rock-water interaction dominance field, confirming that groundwater chemistry is primarily controlled by the dissolution of and interaction with aquifer matrix minerals rather than by atmospheric precipitation or evaporative concentration. This finding is consistent with the humid tropical climate of the study area, where annual rainfall (1,200–1,400 mm) exceeds evaporation, promoting active groundwater recharge. Ion ratios further support this interpretation: Na^+/Cl^- ratios exceeding 1 confirm silicate weathering as the primary sodium source rather than halite dissolution, while remarkably low Cl^-/HCO_3^- ratios (0.02–0.12) confirm meteoric recharge origin with minimal evaporative concentration.

Water quality is compromised by elevated iron concentrations, elevated turbidity, and universal microbial contamination. Iron concentrations ranged from 0.30 to 1.00 mg/L, with 80% of samples exceeding the WHO

(2022) guideline of 0.3 mg/L. Turbidity values ranged from 8.00 to 52.00 NTU, with 70% of samples exceeding the WHO guideline of 5 NTU. Toxic heavy metals (As, Cd, Pb, Hg) were below detection limits (< 0.001 mg/L) in all samples, indicating the absence of industrial pollution and confirming the geogenic stability of the basement complex minerals. Microbiological analysis revealed universal contamination, with all ten samples testing positive for total coliform bacteria (> 180 CFU/100mL), rendering the groundwater unfit for direct consumption without treatment.

The Water Quality Index (WQI) values ranged from 78.91 to 262.84, reflecting considerable spatial variability in groundwater quality across the campus. The WQI classification shows that 40% of samples are classified as "good," 50% as "poor," and 10% as "very poor". The "good" samples (BH1, BH5, BH8, BH10) exhibited relatively lower turbidity and iron concentrations, while the "poor" and "very poor" samples were primarily affected by elevated turbidity, iron, hardness, and in the case of BH7, anomalously high electrical conductivity and total dissolved solids.

Universal microbial contamination poses the most immediate health risk, rendering the groundwater unfit for direct consumption without treatment. All samples require disinfection (chlorination or UV sterilisation) regardless of their chemical WQI classification. The elevated iron and turbidity levels, while primarily geogenic, require treatment to meet aesthetic standards for drinking water. Iron removal via aeration followed by sand filtration is recommended for boreholes exceeding the WHO guideline of 0.3 mg/L Fe, which applies to 80% of the sampled locations. The absence of toxic heavy metals simplifies treatment requirements, allowing efforts to focus on disinfection and iron removal.

This study provides a replicable framework for groundwater quality assessment in crystalline basement terrains and underscores the necessity of routine monitoring, sanitary protection zones, and treatment interventions for sustainable groundwater resource management.

7. RECOMMENDATIONS

7.1 Recommendations for Policy and Practice

Establishment of a Mandatory Water Treatment Protocol: The University management must adopt a compulsory water treatment policy for all boreholes used for drinking and cooking. This should include:

Iron Removal: Aeration and rapid sand filtration systems for boreholes with high iron concentrations (> 0.3 mg/L)

Disinfection: Chlorination (sodium hypochlorite dosing) or UV sterilization systems for all production boreholes

Implementation of Borehole Sanitary Protection Zones: Delineate and enforce a minimum 50-meter sanitary protection radius around each borehole head. Relocate or decommission all potential pollution sources (septic tanks, soak away pits, refuse dumps) within this radius.

Development of a Routine Water Quality Monitoring Program: Implement a quarterly water sampling and analysis program at all functional water points. The minimum analytical suite should include pH, EC, turbidity, total coliforms, E. coli, Fe, and NO_3^-.

Public Health Education and Awareness Campaign: Launch a "Safe Water Initiative" campaign targeting students, faculty, and staff, focusing on safe water handling, storage practices, and reporting of non-functional treatment systems.

7.2 Recommendations for Further Research

Future research should capture temporal variability in water quality across wet and dry seasons to understand seasonal effects on contamination levels.

Isotope Hydrology: Employ stable isotope techniques ($\delta^{18}O$ and $\delta^{2}H$) to precisely determine recharge sources, areas, and mechanisms, and estimate groundwater residence time (Gat, 1996).

Organic Micropollutants: Investigate organic micropollutants (pesticides, pharmaceuticals, personal care products) which were not analyzed in this study.

Health Risk Assessment: Conduct a quantitative microbial risk assessment (QMRA) to evaluate the health risks associated with consuming untreated groundwater from the campus boreholes.

Declarations

Funding:

This research received no external funding.

Clinical Trial Number: Not applicable.

Ethics, Consent to Participate, and Consent to Publish declarations: Not applicable.

Author Contribution

S.M.J. and R.A.A. conceptualized the study and designed the methodology. R.A.A. performed the field investigations, including groundwater sampling, geophysical data acquisition, and pumping tests. R.A.A. conducted the laboratory analyses, including physicochemical, hydrogeochemical, trace metal, and microbiological analyses. R.A.A. processed and interpreted the hydrogeochemical data, including Water Quality Index (WQI) computation, Piper and Gibbs diagram generation, and ion ratio analysis. O.A.O. and S.M.J. supervised the research, provided technical guidance, and validated the analytical results. R.A.A. wrote the original draft of the manuscript. S.M.J. and R.A.A. reviewed and edited the manuscript for intellectual content and scientific rigour. R.A.A. prepared all tables and figures. O.A.O. and S.M.J. provided project administration and resources. All authors reviewed and approved the final version of the manuscript and agree to be accountable for all aspects of the work.

Acknowledgement

The authors thank the Department of Geological Sciences, Osun State University, for providing laboratory and field equipment. The cooperation of the University Works and Maintenance Department in facilitating borehole

access is gratefully acknowledged. We also acknowledge the technical assistance provided by the laboratory staff during sample analysis. The authors thank the anonymous reviewers for their constructive comments, which improved the quality of this manuscript.

Data Availability

The datasets generated and/or analyzed during the current study are available from the corresponding author on reasonable request.

References

1. Adeniran JA, Gbadebo AM, Ojo OM. Water quality index of shallow groundwater in some selected areas of Abeokuta, southwestern Nigeria. Afr J Environ Sci Technol. 2014;8(7):422–8.
2. Adesiyan AB, Akinola AO, Bello AA. Assessment of shallow groundwater quality in parts of Ekiti State using hydrogeochemical and multivariate statistical methods. Nigerian J Environ Sci Technol. 2018;2(1):45–58.
3. Appelo CAJ, Postma D. Geochemistry, groundwater and pollution. 2nd ed. Amsterdam: A.A. Balkema; 2005.
4. Avenbuan N, Omolegan OA, Ikperikpe D. Characterization of subsurface lithological units and aquiferous formations using integrated VLF and VES techniques in Owo, Ondo State. Academy Journal of Science and Engineering; 2025.
5. Boukich O, Bouaissa M, Taupin JD, Patris N, Gharibi E. Groundwater mineralization processes in a semi-arid region: Hydrogeochemical, isotopic and statistical approaches. Groundw Sustainable Dev. 2025;29:101345.
6. Brown RM, McClelland NI, Deininger RA, O'Connor MF. (1972). A water quality index, crashing the psychological barrier. Indic Environ Qual, 173–82.
7. Edet A, Okereke C. Hydrogeologic framework of the shallow aquifers in the basement complex of southeastern Nigeria. Environ Earth Sci. 2014;71(8):3397–412.
8. Ehirim CN, Nwankwo CN. Geoelectric and hydrogeochemical assessment of the groundwater in parts of Port Harcourt, Nigeria. Environ Earth Sci. 2015;73(3):1345–57.
9. Elumalai V, Nkwane RG, Rajmohan N. Evaluation of groundwater quality using water quality index and GIS techniques in parts of the Eastern Cape, South Africa. Environ Earth Sci. 2022;81(3):1–17.
10. Freeze RA, Cherry JA. Groundwater. Englewood Cliffs, NJ: Prentice-Hall; 1979.
11. Gani A, Hussain A, Farooqi A. Groundwater quality assessment using water quality index and principal component analysis in the alluvial plains of the Ganga River basin, India. Environ Monit Assess. 2024;196(2):1–22.
12. Gat JR. Oxygen and hydrogen isotopes in the hydrologic cycle. Annu Rev Earth Planet Sci. 1996;24(1):225–62.
13. Gibbs RJ. Mechanisms controlling world water chemistry. Science. 1970;170(3962):1088–90.
14. Handa BK. Geochemistry and genesis of fluoride-containing ground waters in India. Groundwater. 1975;13(3):275–81.

15. Hem JD. (1985). Study and interpretation of the chemical characteristics of natural water (3rd ed.). U.S. Geological Survey Water-Supply Paper 2254.
16. Hossain MA, Ahmed MK, Sarker SK. Application of water quality index and multivariate statistical techniques to assess groundwater quality in a coastal aquifer of Bangladesh. Groundw Sustainable Dev. 2024;24:101078.
17. Jankowski J, Acworth RI. Impact of debris-flow deposits on hydrogeochemical processes and the development of dryland salinity in the Yass River catchment, New South Wales, Australia. Hydrogeol J. 1997;5(4):71–88.
18. Kumar M, Kumari K, Ramanathan AL. Identification and evaluation of hydrogeochemical processes in the groundwater environment of Delhi. India Environ Geol. 2007;50(7):1025–39.
19. MacDonald AM, Bonsor HC, Dochartaigh BÉ, Taylor RG. Quantitative maps of groundwater resources in Africa. Environ Res Lett. 2012;7(2):024009.
20. Masitoh F, Rusydi AN, Taryana D. Hydrogeochemistry and groundwater quality assessment of shallow groundwater in the Penguluran Basin, East Java, Indonesia. Indonesian J Geoscience. 2025;12(3):343–65.
21. Mukate S, Wagh V, Panaskar D, Jacobs JA, Sawant A. Development of new integrated water quality index (IWQI) model to evaluate the drinking suitability of water. Ecol Ind. 2019;101:348–59.
22. Olobaniyi SB, Owoyemi FB. Characterization by factor analysis of the chemical facies of groundwater in the deltaic plain sand aquifer of Warri, western Niger Delta, Nigeria. Afr J Sci Technol. 2006;7(1):73–81.
23. Olorunfemi MO, Fasuyi SA. Aquifer types and the geoelectric/hydrogeologic characteristics of part of the central basement terrain of Nigeria. J Afr Earth Sc. 1993;16(3):309–17.
24. Piper AM. A graphic procedure in the geochemical interpretation of water analysis. Trans Am Geophys Union. 1944;25(6):914–23.
25. Rahaman MA. Recent advances in the study of the Basement Complex of Nigeria. Precambrian geology of Nigeria. Geological Survey of Nigeria; 1988. pp. 11–41.
26. Ram A, Tiwari SK, Pandey HK, Chaurasia AK, Singh S, Singh YV. Groundwater quality assessment using water quality index (WQI) in parts of Varanasi district, Uttar Pradesh, India. J Geol Soc India. 2021;97(5):521–8.
27. Ramesh K, Elango L. Groundwater quality and its suitability for domestic and agricultural use in Tondiar River Basin, Tamil Nadu, India. Environ Monit Assess. 2012;184(6):3887–99.
28. Salami MB, Ajayi SA, Adewoye AO. Geoelectric investigation of aquifer contamination in a dumpsite in Ibadan, southwestern Nigeria. SpringerPlus. 2016;5(1):1211.
29. Stumm W, Morgan JJ. Aquatic chemistry: Chemical equilibria and rates in natural waters. 3rd ed. New York: Wiley; 1996.
30. Taiwo AM, Gbadebo AM, Azeez MO. Seasonal variation in groundwater quality using water quality index and principal component analysis in Ilesa, southwestern Nigeria. Environ Monit Assess. 2020;192(5):298–312.
31. Tijani MN. Hydrogeochemical assessment of groundwater in Moro area, Kwara State, Nigeria. Environ Geol. 1994;24(3):194–202.
32. Todd DK, Mays LW. Groundwater hydrology. 3rd ed. New York: Wiley; 2005.

33. World Health Organization (WHO). (2024). Guidelines for drinking-water quality (5th ed., incorporating the 1st and 2nd addenda). Geneva: WHO Press.
34. Wright EP. (1992). The hydrogeology of crystalline basement aquifers in Africa. Geological Society, London, Special Publications, 66(1), 1–27.
35. Xu P, Shen Y, Qian H, Zang Y, Liu Y, Peng J. Groundwater quality evaluation and its ecological environmental effects in the Xi'an section of the ecological coordinated control zone at the northern foothills of the Qinling Mountains. Geol Bull China. 2025;44(3):456–70.
36. Xiangxiang C, Lu L, Yutong L, Xueqing Z, Suhua M, Shan L. Chemical characteristics and controlling factors of groundwater in an intensive surface water-groundwater conversion zone: A case study of the Zhengzhou section of the lower Yellow River. Front Environ Sci. 2025;13:1580232.

Figures

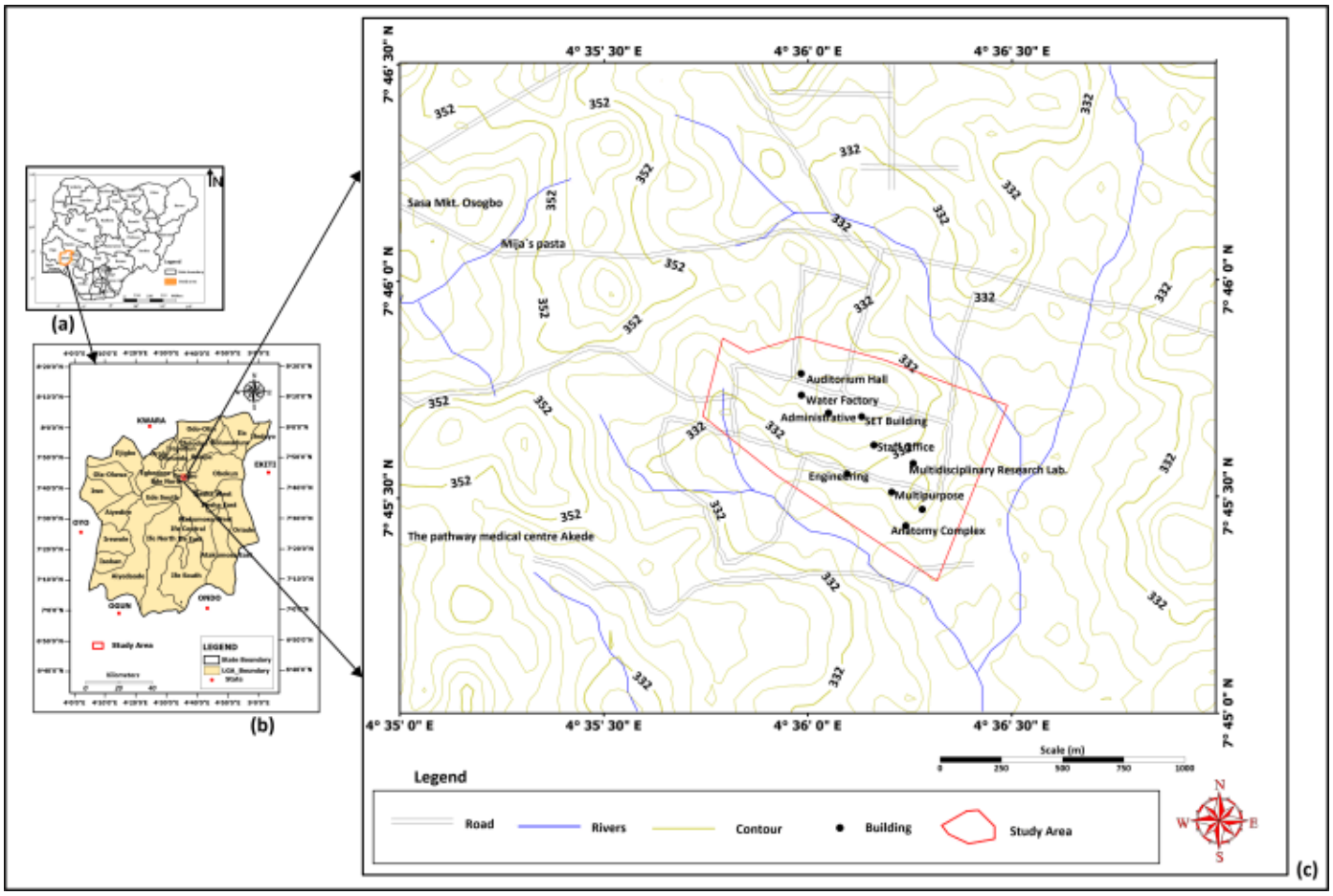


Figure 1

Location Map of the Study Area (culled from Topographical Map of Ilesha NW Sheet 243 1: 50 000 (1965)), the inset is the administrative map of Osun state showing the study area and the Nigeria map.

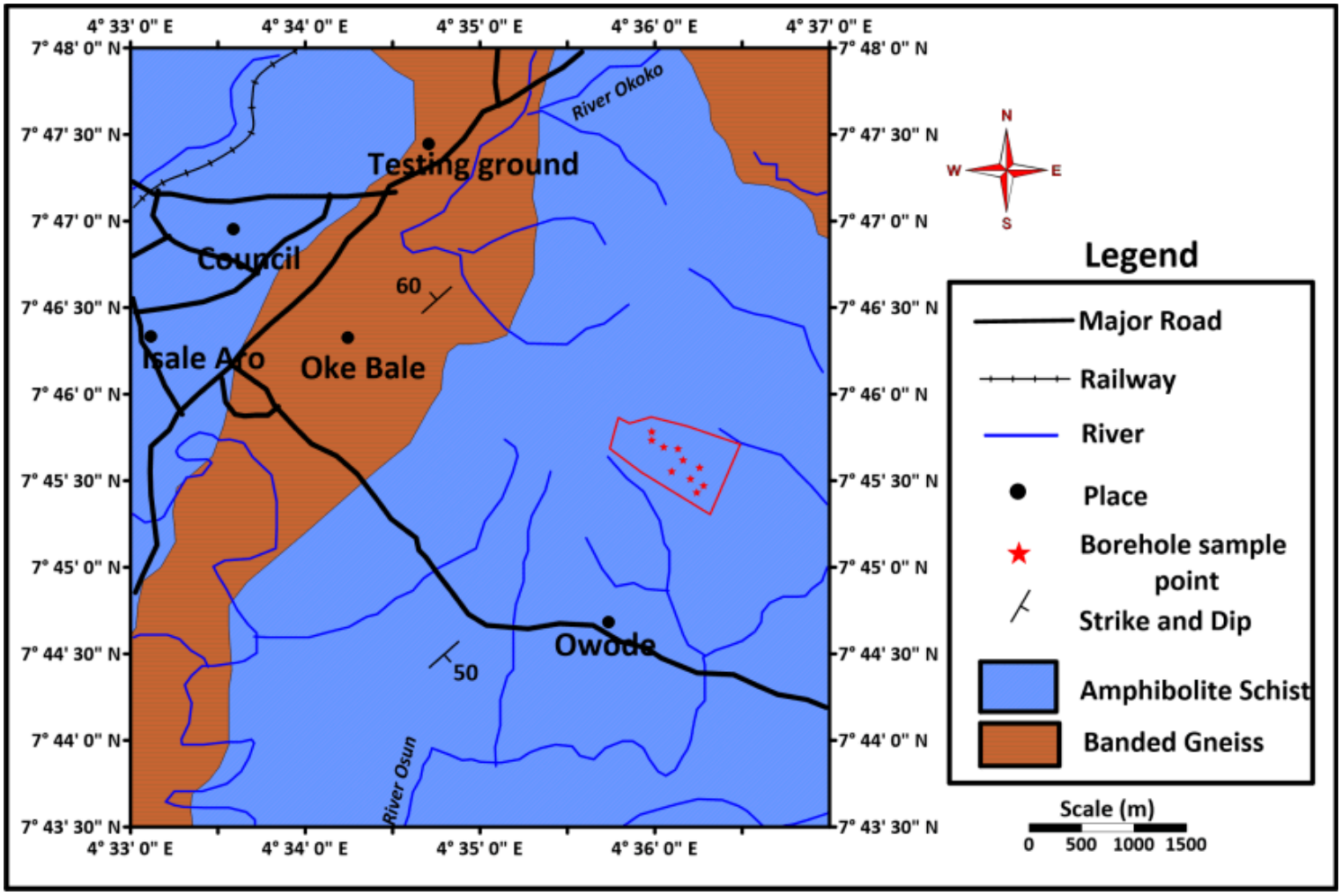


Figure 2

Geological map of the study area, culled from the Geological Map of Osogbo Area (after Bayowa et. al., 2023)

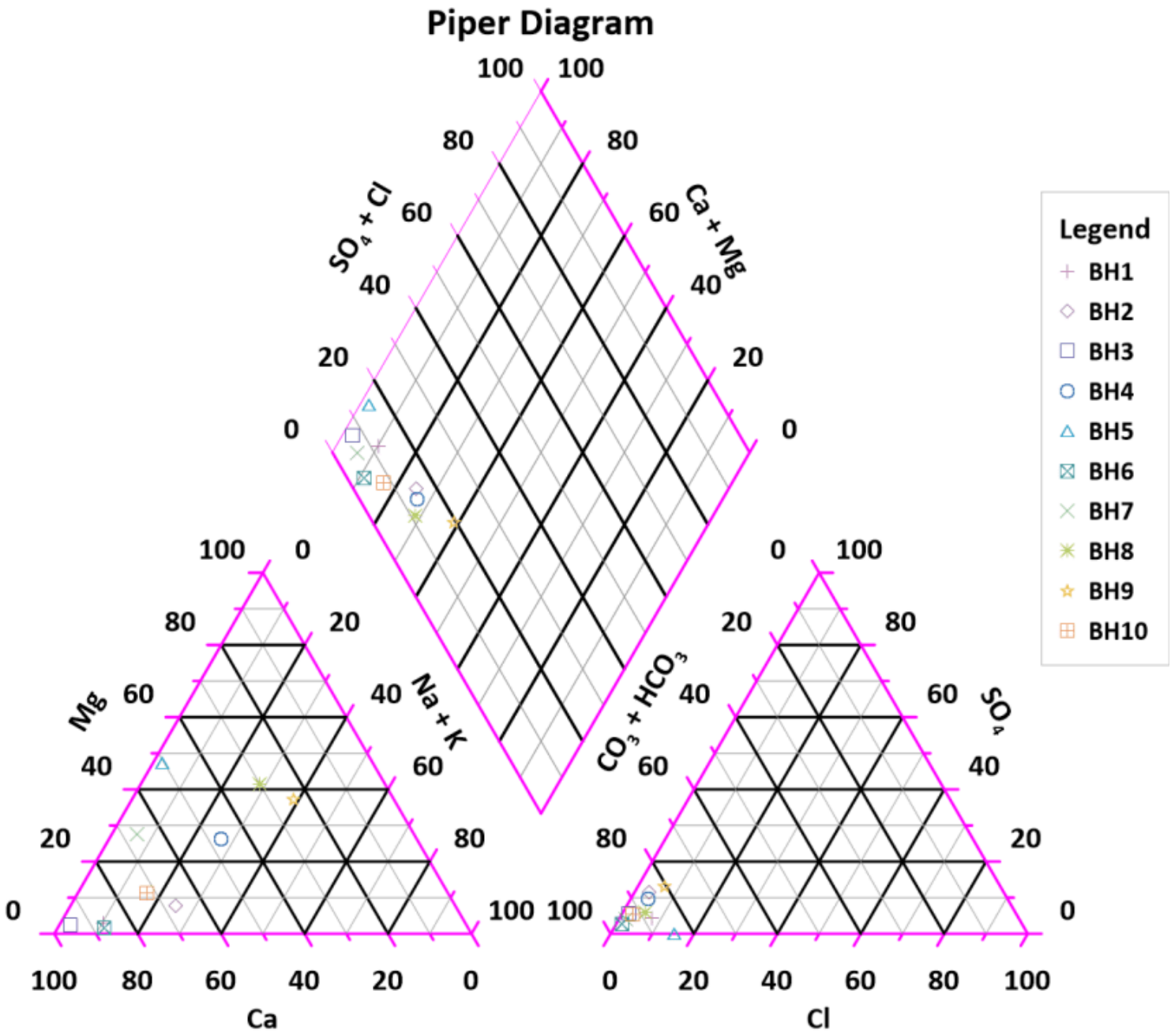


Figure 3

The Piper trilinear diagram showing the hydrogeochemical facies of all ten groundwater samples from the UNIOSUN campus.

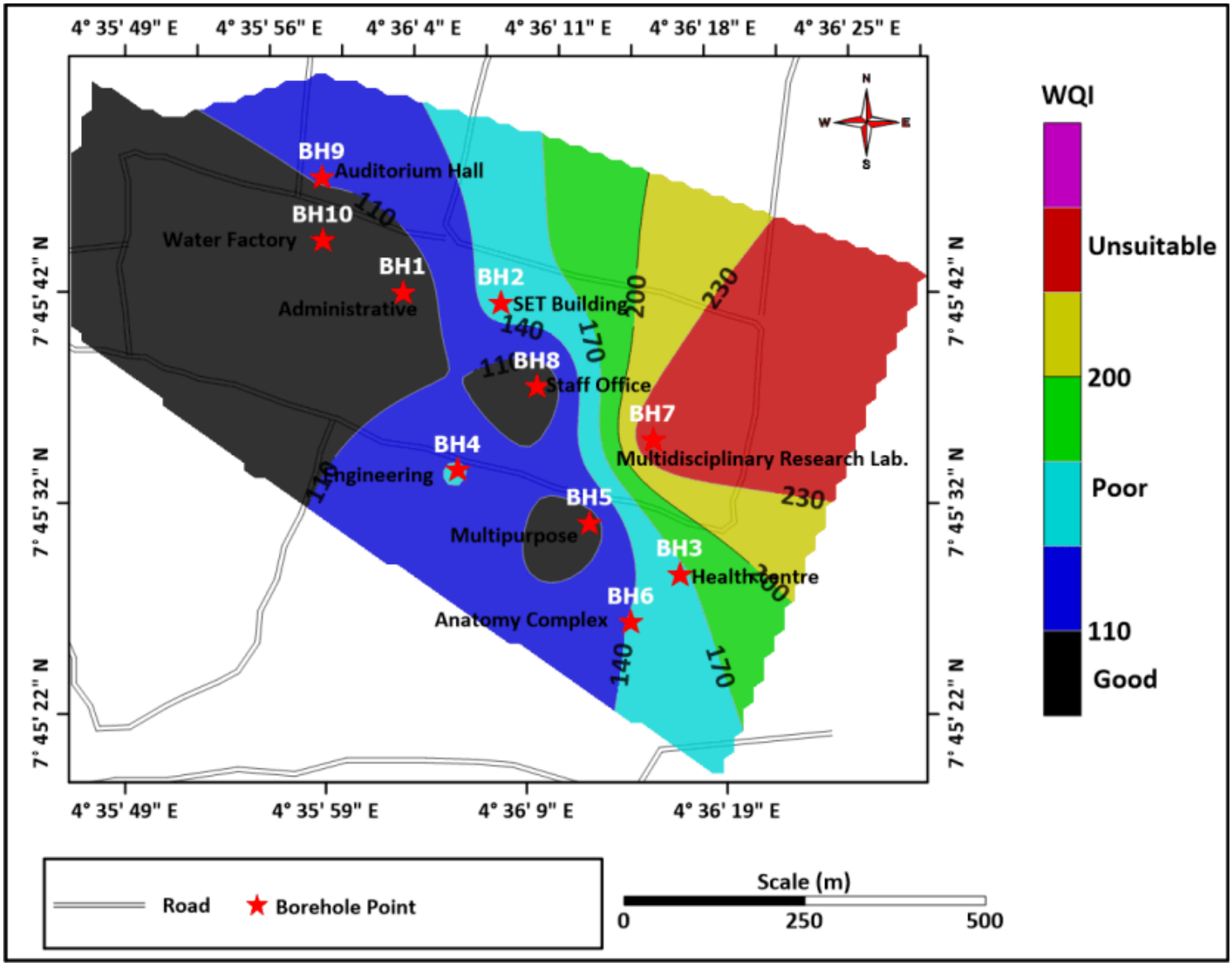


Figure 4

Groundwater Quality map derived from Water Quality Index Distribution Map

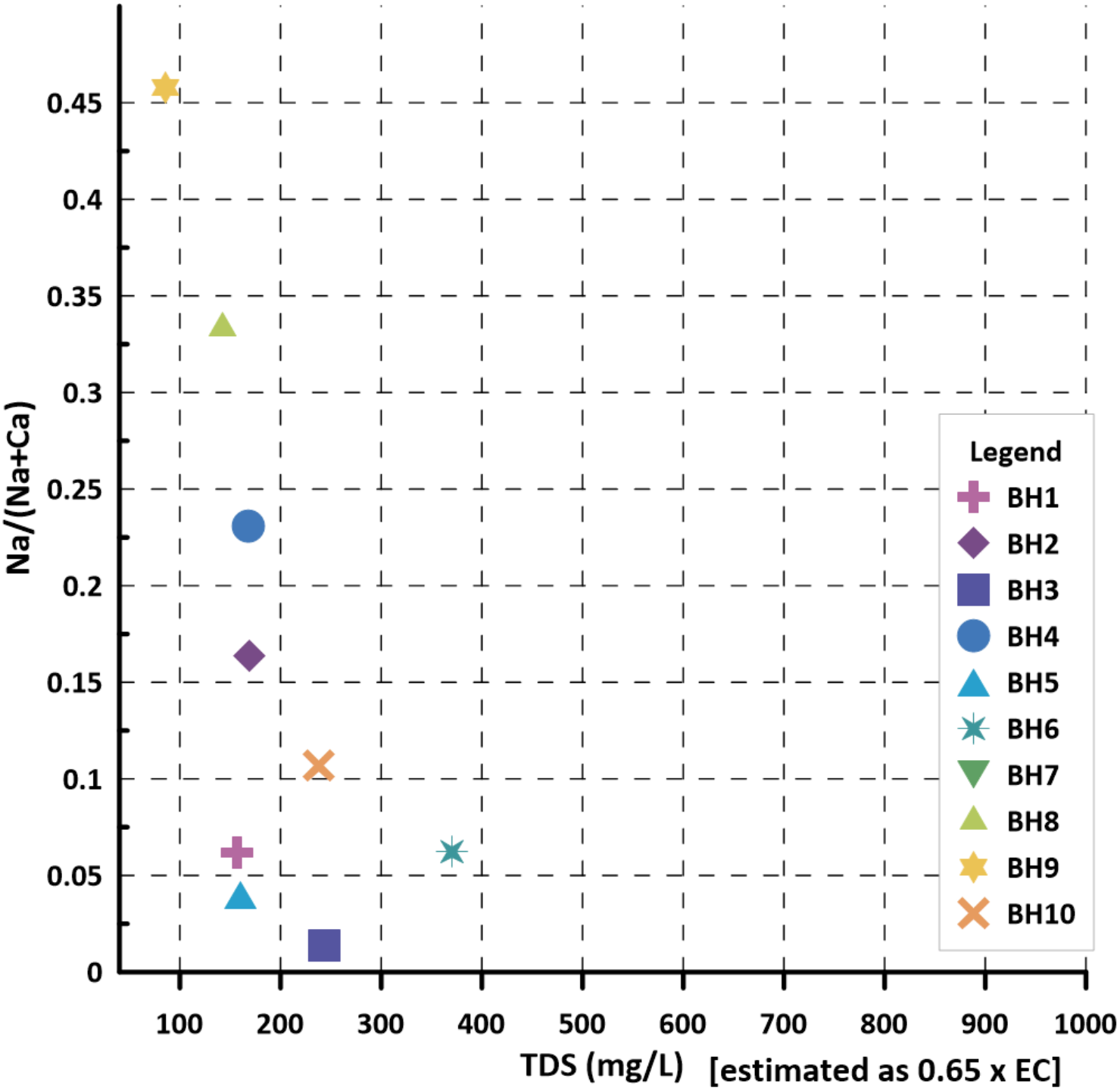


Figure 5

Figure 5(a): The Gibbs Diagram 1 (TDS vs Na/(Na+Ca)

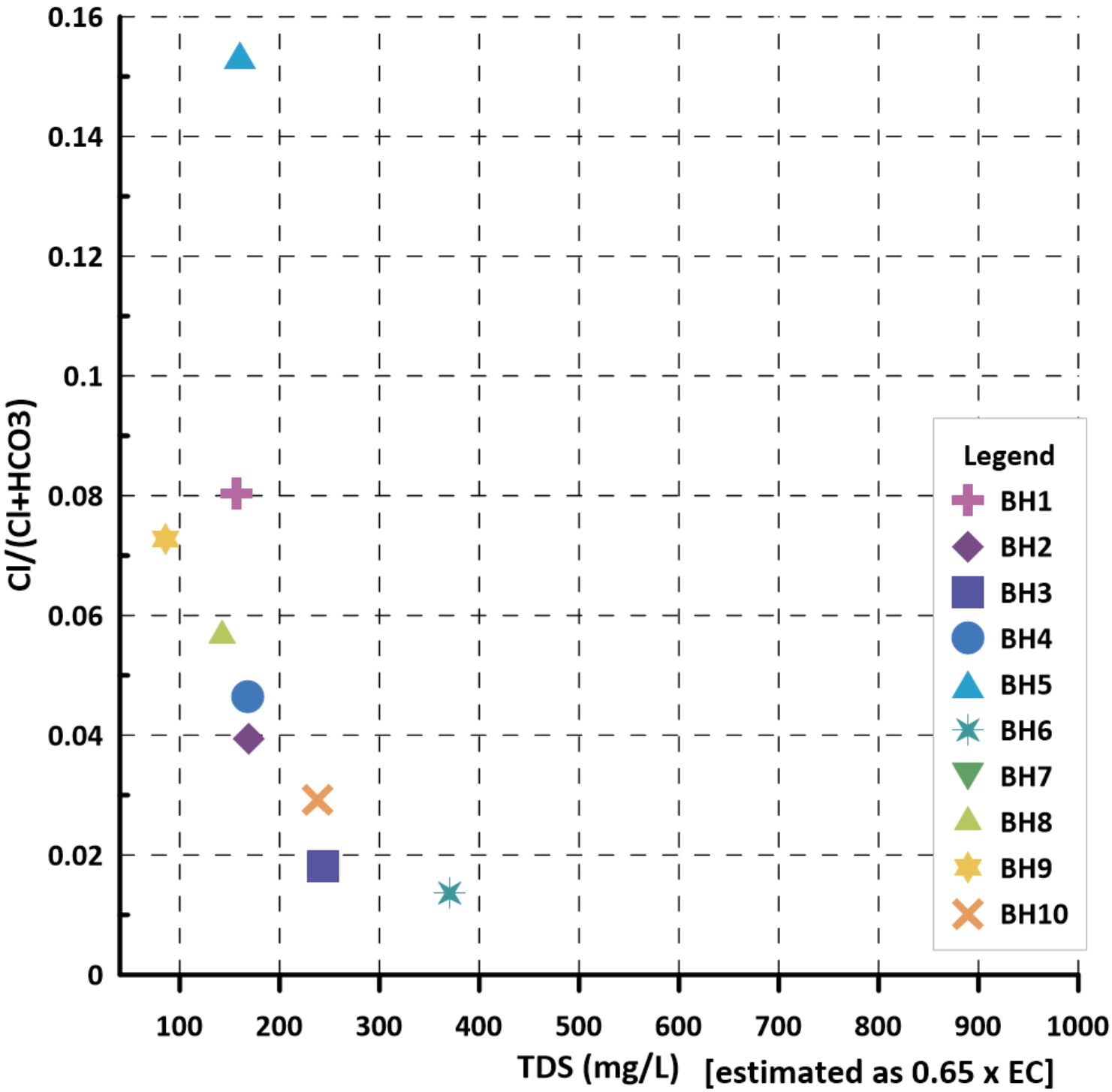


Figure 6

Figure 5(b): The Gibbs Diagram 2 (TDS vs Cl/(Cl+HCO3)

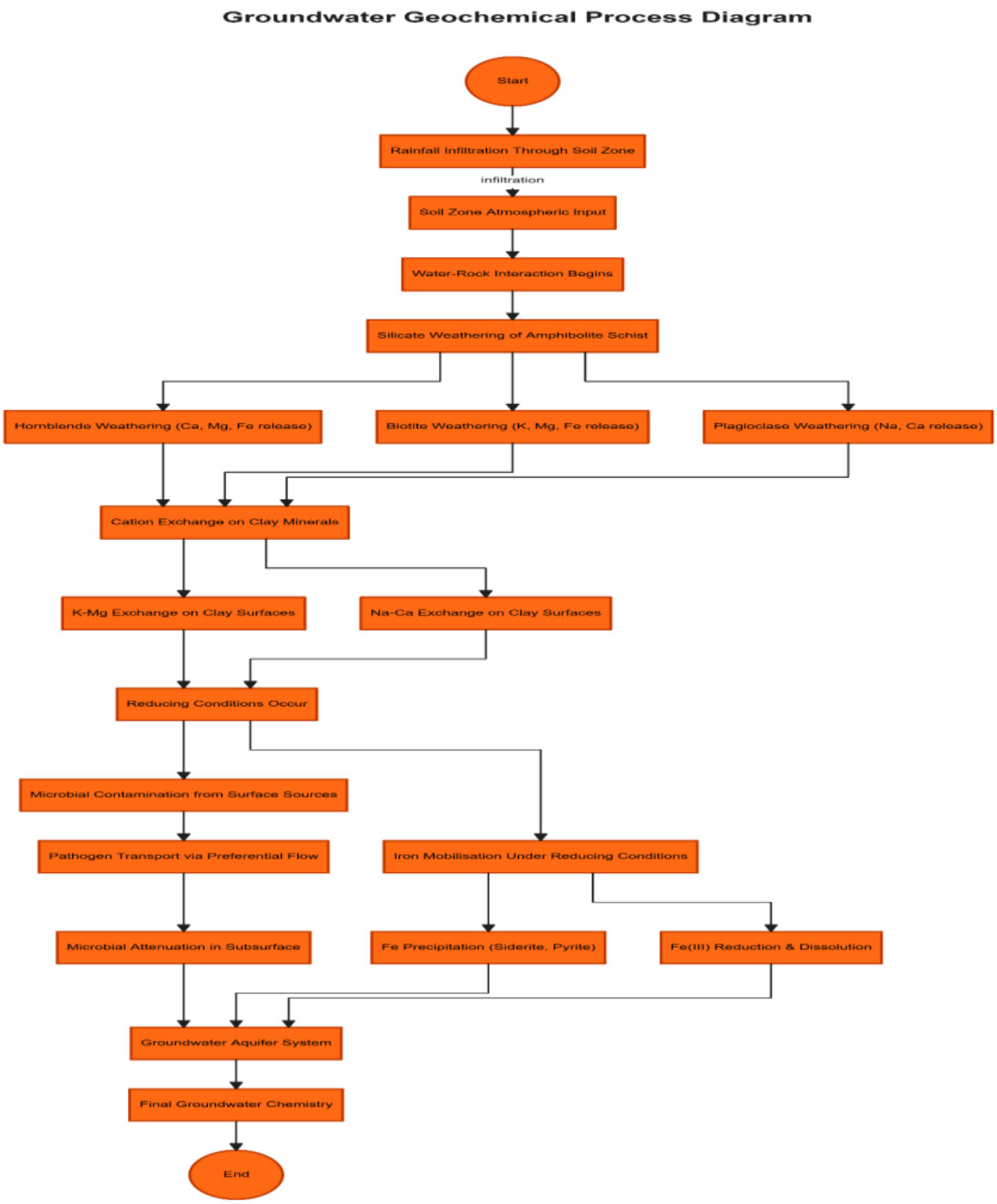


Figure 7

Figure 6: A conceptual diagram (modified after Appelo & Postma, 2005) illustrating the geochemical processes controlling groundwater chemistry in the study area, including: (1) rainfall infiltration through the soil zone, (2) silicate weathering of amphibolite schist (plagioclase, biotite, hornblende), (3) cation exchange on clay minerals, (4) iron mobilisation under reducing conditions, and (5) microbial contamination from surface sources.